EPJ Appl. Metamat. **9**, 13 (2022)

https://doi.org/10.1051/epjam/2022011

EPJ Applied Metamaterials

Available online at:
epjam.edp-open.org

Metamaterials for Novel Wave Phenomena in Microwaves, Optics, and Mechanics

RESEARCH ARTICLE OPEN ACCESS

Free electron harmonic generation in heavily doped semiconductors: the role of the materials properties

Federico De Luca[1,2,*], Michele Ortolani[3,4], and Cristian Ciracì[2]

[1] Istituto Italiano di Tecnologia, Center for Biomolecular Nanotechnologies, Via Barsanti 14, 73010 Arnesano, Italy
[2] Dipartimento di Matematica e Fisica "E. De Giorgi," Università del Salento, via Arnesano, 73100 Lecce, Italy
[3] Department of Physics, Sapienza University of Rome, Piazzale Aldo Moro 5, 00185 Rome, Italy
[4] Istituto Italiano di Tecnologia, Center for Life NanoSciences, Viale Regina Elena 291, 00161 Rome, Italy

Received: 23 October 2021 / Accepted: 1 April 2022

Abstract. Heavily doped semiconductors have emerged as low-loss and tunable materials for plasmonics at mid-infrared frequencies. We analyze the nonlinear optical response of free electrons and show how nonlinear optical phenomena associated with high electron concentration are influenced by the intrinsic properties of semiconductors, namely background permittivity and effective mass. We apply our recently developed hydrodynamic description that takes into account nonlinear contributions up to the third order, usually negligible for noble metals, to compare third-harmonic generation from InP, Ge, GaAs, Si, ITO and InSb. We show how free electron nonlinearities may be enhanced with a proper choice of the semiconductor.

Keywords: Semiconductor plasmonics / infrared photonics / nonlinear optics / hydrodynamic model / third-harmonic generation

1 Introduction

Nonlinear optical phenomena are in general very weak and normally require high laser intensities and long light propagation distances in macroscopic nonlinear crystals to reach operational efficiencies. As a consequence, building integrated nanophotonic platforms based on nonlinear optics can be very challenging. A possibility to face these issues is given by the application of plasmonics to nonlinear optics. Taking advantage of field localization and field enhancement provided by plasmonic modes, one can concentrate and control the light at the nanoscale. Plasmonic nanoantennas made of noble metals are often used as local-field amplifiers in hybrid systems to boost optical nonlinearity from dielectric material placed in their vicinity [1–14]. However, the nonlinear response may also originate directly from the plasmonic material itself and, in particular, from the dynamics of nonequilibrium free electrons (FEs) [15–20]. Nevertheless, high losses, high reflectivity and, sometimes, poor compatibility with the common techniques for nanofabrication used in silicon microelectronics, have limited a widespread application of noble metal plasmonics for practical devices. In this context, heavily doped semiconductors (i.e. with charge densities $n_0 \sim 10^{19} - 10^{20}\,\mathrm{cm}^{-3}$) have been introduced as alternative materials for plasmonic applications [21,22]. Indeed, they can provide lower losses, a tunable optical response (through doping and electrical or optical modulation), and most of them are compatible with large-scale nanofabrication techniques [23].

The first consequence of using heavily doped semiconductors is that the plasma wavelength is in the near-infrared (NIR), i.e., $0.8 < \lambda < 2\,\mu\mathrm{m}$, or in the mid-infrared (MIR), i.e., $2 < \lambda < 20\,\mu\mathrm{m}$, λ being the free-space wavelength. This opens a new realm of applications for plasmonics, for example, in sensing, due to the overlap with the so-called molecular fingerprint spectrum [23], and in free-space telecommunications, since the 3–5 μm and the 8–13 μm atmospheric transparency windows are less affected by atmospheric turbulence, clouds and fog [24]. It will be shown later in this work that third order FE nonlinearities are inversely proportional to the square of the charge density, and, since the values of charge density in heavily doped semiconductors are three orders of magnitude smaller than in noble metals, another consequence of a long plasma wavelength is that third-order nonlinear effects can be up to six orders of magnitude larger in doped semiconductors if compared to traditional plasmonic metals.

We recently used a hydrodynamic model to describe FE nonlinear optical dynamics in heavily doped semiconductors, investigating FE contributions to the third-harmonic

* e-mail: federico.deluca@iit.it

generation (THG) process through the derivation of nonlinear hydrodynamic terms up to the third order. We have shown that, contrarily to noble metals at optical frequencies, THG in heavily doped semiconductor is predicted to be strongly driven by hydrodynamic nonlinearities and that cascaded contributions might be extremely important [25].

In our previous work we considered a single semiconductor, indium phosphide (InP), focusing our analysis on the development and on the physical predictions of the model. However, the large variety of semiconductors with different effective electron mass and doping levels gives access to a wide range of possibilities to optimize and increase intrinsic nonlinear effects. In this article, going toward a practical application of the concept, we complement our study on FE nonlinearities in heavily doped semiconductors, comparing the THG efficiencies of several semiconductors, namely InP, germanium (Ge), gallium arsenide (GaAs), silicon (Si), indium thin oxide (ITO) and indium antimonide (InSb), in order to show how the properties of the material may influence the harmonic generation.

2 Model

To describe nonlinear light-matter interactions in a FE gas like in heavily doped semiconductors (but also in noble metals), one needs to couple a constitutive relation that describes the intrinsic nonlinear dynamics of the electrons to the wave equation. Within the hydrodynamic formalism [26–28], the many-body dynamics of a FE fluid, under the influence of external electric- and magnetic-fields $\boldsymbol{E}(\boldsymbol{r},t)$ and $\boldsymbol{H}(\boldsymbol{r},t)$, can be described by the following equation:

$$\frac{\partial \boldsymbol{J}}{\partial t}+\gamma \boldsymbol{J}=\frac{e^2 n}{m}\boldsymbol{E}-\frac{\mu_0 e}{m}\boldsymbol{J}\times\boldsymbol{H}+\frac{1}{e}\left(\frac{\boldsymbol{J}}{n}\nabla\cdot\boldsymbol{J}+\boldsymbol{J}\cdot\nabla\frac{\boldsymbol{J}}{n}\right)+\frac{en}{m}\nabla\frac{\delta T^{TF}[n]}{\delta n} \tag{1}$$

where m is the electron effective mass, e the elementary charge (in absolute value), μ_0 is the magnetic permeability of vacuum and γ is the damping rate. In this equation two macroscopic variables are considered, the charge-density $n(\boldsymbol{r},t)$, and the current density $\boldsymbol{J}(\boldsymbol{r},t)=-en\boldsymbol{v}$, with $\boldsymbol{v}(\boldsymbol{r},t)$ being the electron velocity field. The last term in equation (1) takes into account the nonlocal effects due to the quantum pressure. Indeed, $T^{TF}[n]$ is the kinetic-energy functional in the Thomas-Fermi (TF) approximation, whose functional derivative with respect to n is $\frac{\delta T^{TF}[n]}{\delta n}=\frac{5}{3}c_{TF}n^{\frac{2}{3}}$, with $c_{TF}=\frac{\hbar^2}{m}\frac{3}{10}(3\pi^2)^{\frac{2}{3}}$ [29]. The introduction of an electron pressure term in the FE model accounts for the fermionic nature of the charge carriers, which cannot be compressed in an infinitesimally thin layer. However, within the TF approximation, the equilibrium charge density n_0 is assumed to be constant inside the semiconductor and abruptly go to zero outside. This is not necessarily true in correspondence of the semiconductor surface, where there can be small variations of the density. In any case, we assume that these effects can be neglected. In addition, we neglect electron spill-out and apply hard-wall boundary conditions.

Following a perturbative approach and expanding all the fields up to the third order as described in reference [25], the nonlinear response of FEs in heavily doped semiconductors, i.e. equation (1), can be rewritten taking into account the polarization field $\boldsymbol{P}(\boldsymbol{r},t)$ as follows:

$$\ddot{\boldsymbol{P}}+\gamma\dot{\boldsymbol{P}}=\frac{n_0e^2}{m}\boldsymbol{E}+\beta^2\nabla(\nabla\cdot\boldsymbol{P})+\boldsymbol{S}_{NL}^{(2)}+\boldsymbol{S}_{NL}^{(3)} \tag{2}$$

where $\dot{\boldsymbol{P}}=\boldsymbol{J}$, with time derivatives are expressed in dot notation. Here, $\beta^2=\frac{10}{9}\frac{c_{TF}}{m}n_0^{\frac{2}{3}}$, while $\boldsymbol{S}_{NL}^{(2)}$ and $\boldsymbol{S}_{NL}^{(3)}$ are the second- and third-order nonlinear sources, whose expressions are

$$\boldsymbol{S}_{NL}^{(2)}=\frac{e}{m}\boldsymbol{E}\nabla\cdot\boldsymbol{P}-\frac{e\mu_0}{m}\dot{\boldsymbol{P}}\times\boldsymbol{H}+\frac{1}{en_0}\left(\dot{\boldsymbol{P}}\nabla\cdot\dot{\boldsymbol{P}}+\dot{\boldsymbol{P}}\cdot\nabla\dot{\boldsymbol{P}}\right)+\frac{1}{3}\frac{\beta^2}{en_0}\nabla(\nabla\cdot\boldsymbol{P})^2, \tag{3}$$

$$\boldsymbol{S}_{NL}^{(3)}=-\frac{1}{e^2n_0^2}\left(\nabla\cdot\boldsymbol{P}(\dot{\boldsymbol{P}}\nabla\cdot\dot{\boldsymbol{P}}+\dot{\boldsymbol{P}}\cdot\nabla\dot{\boldsymbol{P}})+\dot{\boldsymbol{P}}\cdot\dot{\boldsymbol{P}}\nabla\nabla\cdot\boldsymbol{P}\right)-\frac{1}{27}\frac{\beta^2}{e^2n_0^2}\nabla(\nabla\cdot\boldsymbol{P})^3. \tag{4}$$

Assuming harmonic fields within the undepleted pump approximation and coupling the previous expressions to Maxwell's wave equation, as described in reference [25], full sets of hydrodynamic equations can be derived for the specific nonlinear process of interest. We solved these equations numerically using the finite-element method within a customized frequency-dependent two-dimensional implementation in COMSOL MULTIPHYSICS [30].

3. Preliminary discussion

Let us consider the THG process, in which a signal oscillating at 3ω is generated from a pump field at ω after its nonlinear interaction with the medium. To investigate the THG arising from FE nonlinearities in heavily doped semiconductors, we study a plain geometry, namely a 1 μm thick slab, for simplicity in air. On top of the Drude-like dispersion described by equation (2), we consider a local permittivity contribution, ε_∞, in the semiconductor linear response, such that, neglecting nonlocal effects, we retrieve the usual dielectric function $\varepsilon(\omega)=\varepsilon_\infty-\frac{\omega_P^2}{\omega^2+i\gamma\omega}$, where $\omega_P=\sqrt{\frac{e^2n_0}{\varepsilon_0 m}}$ is the plasma frequency of the material, being ε_0 the dielectric constant of vacuum. As it can be seen in Figure 1, we consider a plane wave impinging on the geometry with a certain angle of incidence θ. For the sake of simplicity, we only consider reflected THG, while the pump peak intensity is $I_0=10\,\frac{W}{\mu m^2}\left(1\,\frac{GW}{cm^2}\right)$, that corresponds to an input electric field of $E_0=8.7\times10^7$ V/m, a value that can be obtained with a commercial difference-frequency generation source based on ultra-fast laser pulses, and that is also close to the estimated breakdown fields of heavily doped semiconductors. The THG efficiency can be obtained by normalizing the power of the generated signal to the input power at the fundamental frequency

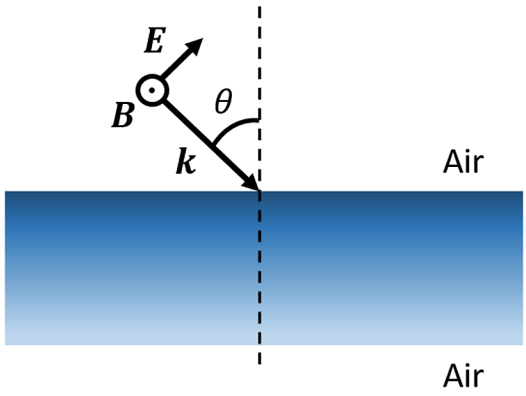

Fig. 1. Schematics of the studied geometry: a transverse magnetic mode impinging on a slab of highly doped semiconductor with an angle of incidence θ. The simulated slab is assumed to be in air and 1 μm thick.

$\eta = I_G/I_0$, where I_G is the generated intensity. Since we are considering third-order nonlinearities, I_G is expected to be proportional to I_0^3, therefore η will scale with I_0^2.

In Figure 2d we report the curves for the efficiencies η obtained when all the contributions to THG are taken into account. These include hydrodynamic (direct and cascaded) and intrinsic nonlinearities. The other plots refer to isolated nonlinear sources, discussed as follows. Figure 2a is obtained by taking into account only the third order hydrodynamic nonlinear source term, i.e. equation (4). All the terms in equation (4) are surface-like terms, because they depend on the divergence of the polarization. As it can be seen in Figure 2a, the efficiency is zero at normal incidence and it grows with the angle of incidence, peaking at around 70°. This is due to the fact that, at normal incidence, the electric field is parallel to the slab, as a consequence there cannot be oscillations in the finite dimension of the slab and the THG field is then zero. However, the process that we have just discussed is not the only way to generate a signal at 3ω starting from a signal at ω. Indeed, it is also possible to have what is called, cascaded THG, a combination of two second order processes. In this case, two photons at ω first combine through a second harmonic generation (SHG) process to generate an output at 2ω, this then combines with the input at ω to give a signal at 3ω through sum frequency generation. It should be noted that second order processes are forbidden in centrosymmetric materials, and can only occur at the material surface, where the symmetry is broken. This is not entirely true in heavily doped semiconductors, thanks to the rich nonlinear dynamic of FEs [31–34]. Indeed, one can observe cascaded THG originating in the FE gas according to the second order nonlinear source, equation (3). A very important feature, discussed in references [25,34], is that, at normal incidence, even if the SHG efficiency is zero, the cascaded THG is not zero, see Figure 2b (FE-cascaded). To understand this point, notice that the second order nonlinear source contains not only surface terms, therefore not exclusively terms that depend on the divergence of the polarization field, but it also contains bulk terms, such as the Lorentz term, proportional to $\boldsymbol{P} \times \boldsymbol{H}$. As a consequence, at normal incidence, for a fundamental field parallel to the slab, its cross product with the magnetic field gives a second harmonic field that is perpendicular to the geometry. This signal, even if is not visible in the far-field (since it cannot couple to the free-space transverse modes, giving zero SHG efficiency at normal incidence), can interact with the FE gas in the slab to give a non-zero cascaded signal. Finally, the efficiencies related to THG originating in the background lattice, due to the intrinsic third-order nonlinear susceptibility $\chi^{(3)}$ (tensor's highest component) of each material are calculated as in reference [25] and are reported in Figure 2c.

The background permittivity, ε_∞, the effective mass, the screened plasma wavelength $\tilde{\lambda}_P$ and the third-order nonlinear susceptibility of the materials analyzed are reported in Table 1.

Here, $\tilde{\lambda}_P = \frac{2\pi c}{\tilde{\omega}_P}$, with $\tilde{\omega}_P = \frac{\omega_P}{\sqrt{\varepsilon_\infty}}$ being the screened plasma frequency and c is the speed of light. For all the semiconductors, the level of doping is fixed to $n_0 = 10^{20}\text{cm}^{-3}$ (all the plasma wavelengths are in the MIR or in the NIR), $\gamma = 10\,\text{ps}^{-1}$, while the wavelength of the fundamental field (FF) is $\lambda_{FF} = 3.2\tilde{\lambda}_P$. The coefficient 3.2 is the minimum factor that can be chosen in order to have all the harmonics in the metallic region of the materials and the TH far enough from the condition of epsilon near zero, that would cause an enhancement of the hydrodynamic nonlinearities, as discussed in references [25,34].

4 Results

Analyzing the hydrodynamic THG efficiencies in Figure 2, it can be observed that, in the case of FE direct contributions (Fig. 2a), the material reaching the highest value for a given angle of incidence is ITO (red line), the following is InP (orange line), then, in order, GaAs (black line), Si (blue line), Ge (green line) and InSb (light blue line). This is coherent with the color map in Figure 2e, in which the efficiency of FE direct THG is reported as a function of ε_∞ and m, for a fixed θ, and where η decreases with an increasing ε_∞, while it stays nearly steady with m. Indeed, ITO has the smallest ε_∞, then follow InP, GaAs, Si, InSb, and Ge. This behavior is due to the fact that, for a given angle of incidence, a higher ε_∞ causes the transmitted FF at the interface air/semiconductor to refract a smaller angle when propagating inside the slab. Because surface contributions are hindered at near-normal incidence, the FE direct THG efficiency, due only to surface contributions, becomes smaller when increasing ε_∞ [25]. However, the trend is blurred for very small effective masses, when nonlocal effects becomes very large and cause a sharp decrease of the surface effects and, hence, of the efficiency, as in the case of InSb.

Let us now compare the efficiencies in the case of cascaded nonlinearities (Fig. 2b). Here, both ε_∞ and m play a central role. For instance, let us focus on Si, which, as

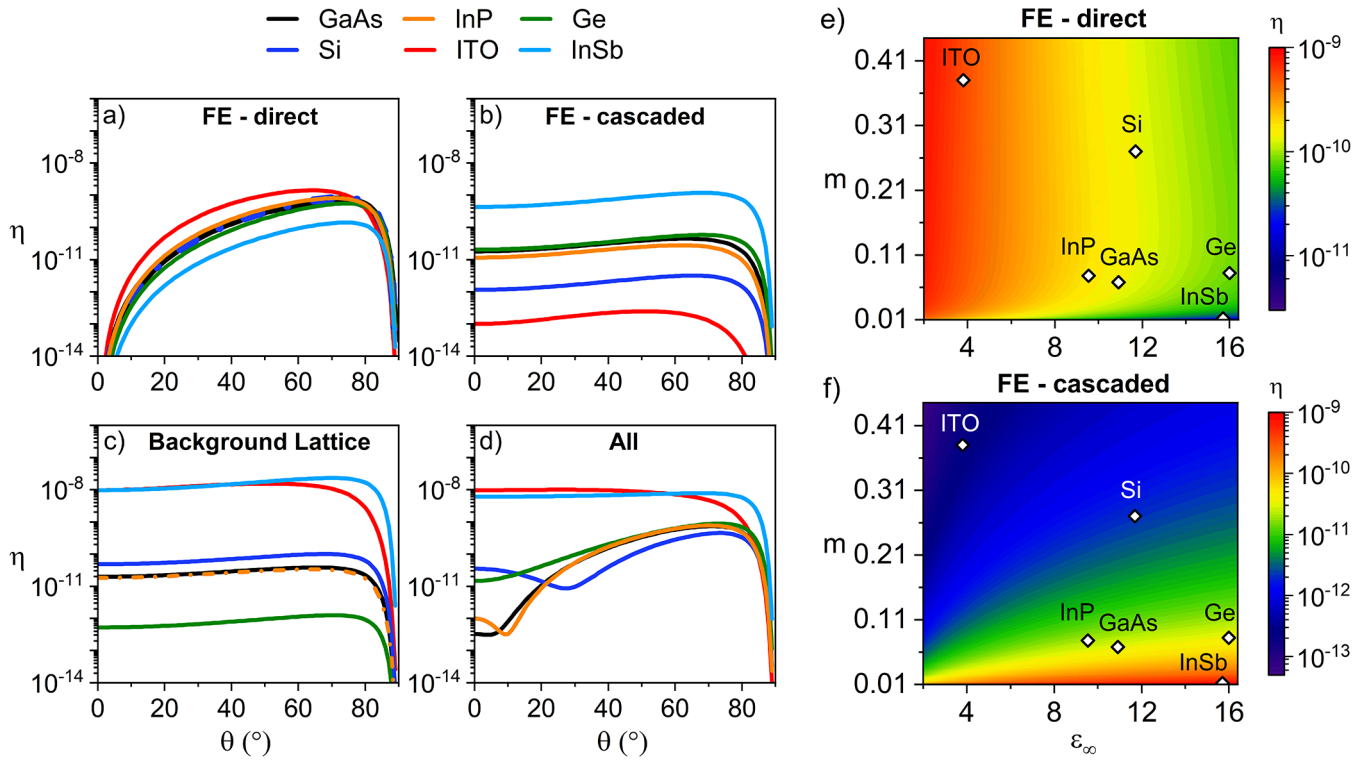

Fig. 2. (a–d) THG efficiency η of the highly doped semiconductor slab as a function of the incident angle θ and for different materials. Data reported in plots (a–c) are calculated taking into account distinct nonlinear sources: (a) is obtained considering only FE direct contributions; (b) refers to the FE cascaded THG; (c) to the THG originating from background lattice third-order susceptibility $\chi^{(3)}$. In plot (d) the curves are those predicted for a real experiment where all the contributions to THG are taken into account. (e–f) η as a function of the background permittivity, ε_∞, and of the effective mass, m, for a fixed angle of incidence $\theta = 40°$ in the case of FE-direct (e) and FE-cascaded (f) THG. Here, white diamond represent the semiconductors studied in correspondence of their values of ε_∞ and m. The level of doping and the wavelength of the fundamental field (FF) are fixed to $n_0 = 10^{20}\text{cm}^{-3}$ and $\lambda_{FF} = 3.2\tilde{\lambda}_P$, respectively, in all plots.

Table 1. The materials studied and their properties.

Semiconductor	ε_∞	m	$\tilde{\lambda}_P(\mu\text{m})$	$\chi^{(3)}(\times 10^{-18}\text{m}^2/\text{V}^2)$
ITO	3.80 [22]	0.380 [22]	4.0	3.3 [37]
InP	9.55 [22]	0.078 [22]	2.9	1.0 [25]
GaAs	10.91 [22]	0.068 [22]	2.9	1.4 [35]
Si	11.70 [22]	0.270 [22]	5.9	2.8 [35]
InSb	15.7 [38]	0.012 [38]	1.5	70.0 [39]
Ge	16.00 [36]	0.082 [36]	3.8	0.56 [35]

already mentioned, has the second highest ε_∞. As a consequence, it should be expected to reach the second highest THG efficiency since the presence of the Lorenz term in the second order nonlinear source should drive the increase of THG efficiency with the background permittivity value [25]. Nevertheless, its cascaded THG efficiency is the smallest after that of ITO. To solve this conundrum, les us consider the color map in Figure 2f, in which the efficiency of FE cascaded THG is reported as a function of ε_∞ and m, for a fixed θ. As it can be noticed, high background permittivities and small effective masses favor FE cascaded nonlinearities. The trend with respect to m can be intuitively understood considering the explicit dependence of the second order hydrodynamic source on the effective mass in equation (3). This explains why the cascaded THG efficiency of Si, which has a background permittivity comparable with those of InP and GaAs, but has an effective mass at least three times larger, is one order of magnitude smaller than that of the other two semiconductors. The efficiency of ITO is instead limited because this semiconductor has both the smallest ε_∞ and the highest m, contrarily to InSb, which reaches the highest efficiency thanks to the smallest m and a very high ε_∞. Considering Figure 2c, the differences between the curves

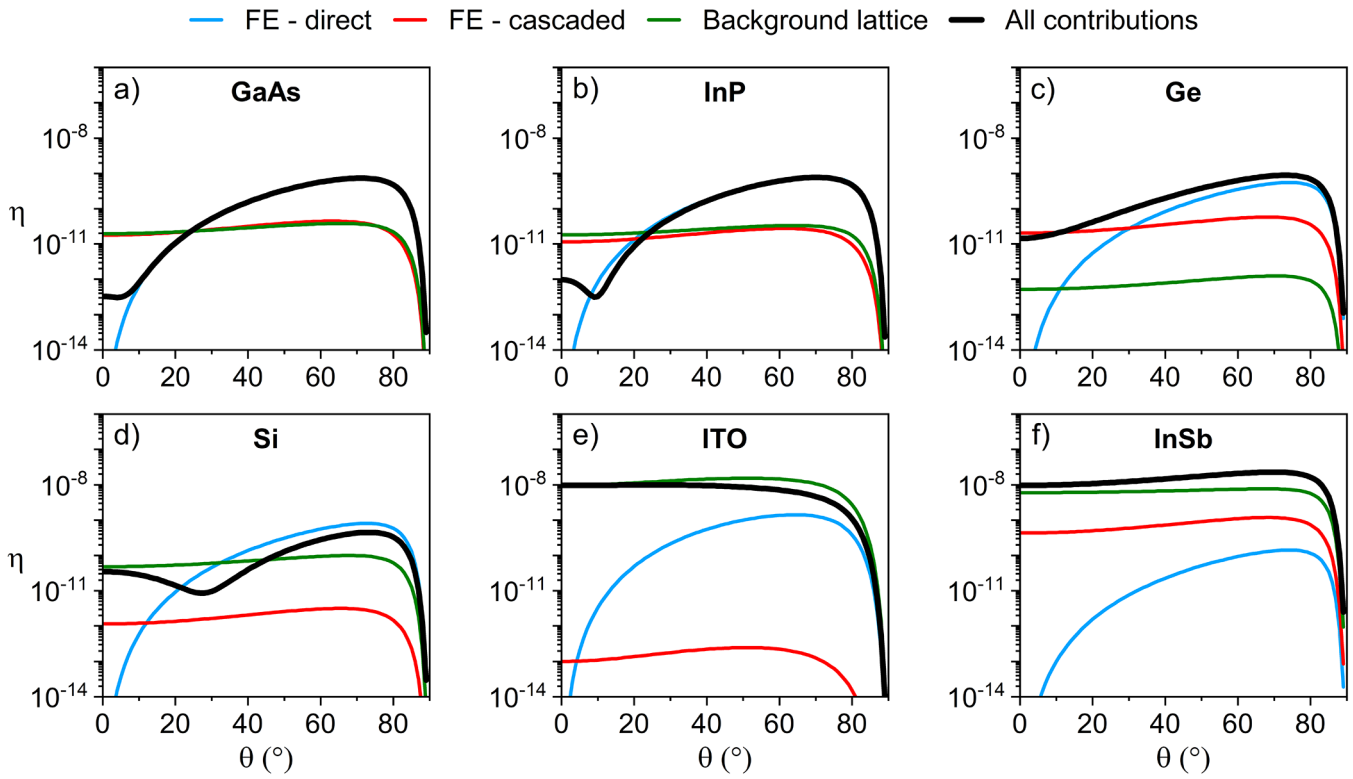

Fig. 3. THG efficiency η of a highly doped semiconductor slab as a function of the incident angle θ and for the different nonlinear sources, organized by material. Plots (a)–(f) take into account GaAs, InP, Ge, Si, ITO, and InSb respectively.

of efficiency of THG originating from the crystalline lattice of the semiconductors are apparently due to the distinct values of third order nonlinear susceptibility, indeed InSb and ITO have the highest $\chi^{(3)}$, then follow Si, GaAs, InP and Ge. However, this does not completely explain the quantitative differences in the absolute values of the efficiencies, that, from their definition, one would expect to scale as $\eta \propto \chi^{(3)\wedge}2$. For instance, since $\chi^{(3)}_{InSb} \approx 21\chi^{(3)}_{ITO}$ and $\chi^{(3)}_{ITO} = 3.3\chi^{(3)}_{InP}$, one would predict the efficiency of ITO, η_{ITO}, to be more than 400 time smaller than that of InSb, η_{InSb}, and about 10 times larger if compared to the efficiency of InP, η_{InP}. Nevertheless, from Figure 2c, $\eta_{ITO} \approx \eta_{InSb}$ for a wide range of angles of incidence and $\eta_{ITO} \approx 1000\eta_{InP}$.This differences between the calculated and the expected ratios may be explained considering also in this case the role of the background permittivity. Indeed, for background lattice nonlinearities, η is higher for lower ε_∞ because of the higher transparency of the material [25]. This makes it clear as well why InP and GaAs have essentially the same maximum efficiency even if $\chi^{(3)}_{InP} \approx 1.4\chi^{(3)}_{GaAs}$ and why the background lattice THG efficiency of ITO is more than 100 times larger than that of Si notwithstanding the fact that $\chi^{(3)}_{ITO} \sim 1.2\chi^{(3)}_{Si}$.

At this point, it should be easier to understand the features in the plot of Figure 2d, where all nonlinear contributions are taken into account simultaneously. To make the peculiar characteristics of every material even more clear, we report in Figure 3 the same data of Figure 2 organized by material. In the case of ITO, the very large background lattice nonlinear effects dominate for all the angles of incidence. The same can be observed for InSb, however, here cascaded nonlinearities have a role in increasing the total efficiency. Instead, for all the other semiconductors the trend at higher angle of incidence is due to FE nonlinearities, while, at normal incidence, it depends on the reciprocal order of magnitude of cascaded and background lattice THG efficiencies. For instance, considering Ge, the former contribution prevails, while the latter contribution dominates for Si. Instead, when considering InP and GaAs, the cascaded and intrinsic nonlinearities are of the same order and interfere destructively. A similar interference can be finally observed between FE direct and intrinsic THG at high angles for ITO and Si.

5 Conclusions

We have applied our recently developed hydrodynamic formalism for the description of FE nonlinear dynamics in heavily doped semiconductors to investigate how the choice of the semiconductor may influence the nonlinear optical phenomena associated with a high concentration of FEs. Through the numerical study of FE contributions to the process of THG from a semiconductor slab, we have compared the efficiency of harmonic generation of several materials, and we have shown that their intrinsic properties can cause a difference of several order of magnitude in the efficiency of THG both in the case of FE and background lattice nonlinearities. In particular, we have

found that, at normal incidence, the role of FE nonlinearities in determining the total nonlinear optical response of a doped semiconductor is crucial in small effective mass semiconductors such as n-doped InSb, GaAs, and InP, while, at high angles of incidence, it is relevant for the semiconductors with the highest background permittivities (GaAs, Ge and Si). Indeed, FE nonlinearities are almost negligible in materials like ITO, characterized by the highest effective mass and the smallest background permittivity, the latter causing a high enhancement of background lattice nonlinear effects.

References

1. Q. Shen, W. Jin, G. Yang, A.W. Rodriguez, M.H. Mikkelsen, Active control of multiple, simultaneous nonlinear optical processes in plasmonic nanogap cavities, ACS Photonics **7**, 901 (2020)
2. R. Sarma, D. de Ceglia, N. Nookala, M.A. Vincenti, S. Campione, O. Wolf, M. Scalora, M.B. Sinclair, M.A. Belkin, I. Brener, Broadband and efficient second-harmonic generation from a hybrid dielectric metasurface/semiconductor quantum-well structure, ACS Photonics **6**, 1458 (2019)
3. Y. Zeng, H. Qian, M.J. Rozin, Z. Liu, A.R. Tao, Enhanced second harmonic generation in double-resonance colloidal metasurfaces, Adv. Funct. Mater. **28**, 1803019 (2018)
4. A.R. Echarri, J.D. Cox, R. Yu, F.J.G. de Abajo, Enhancement of nonlinear optical phenomena by localized resonances, ACS Photonics **5**, 1521 (2018)
5. Q. Shen, T.B. Hoang, G. Yang, V.D. Wheeler, M.H. Mikkelsen, Probing the origin of highly-efficient thirdharmonic generation in plasmonic nanogaps, Opt. Express **26**, 20718 (2018)
6. S. Guddala, S.A. Ramakrishna, Optical limiting by nonlinear tuning of resonance in metamaterial absorbers, Opt. Lett. **41**, 5150 (2016)
7. T. Shibanuma, G. Grinblat, P. Albella, S.A. Maier, Efficient third harmonic generation from metal – dielectric hybrid nanoantennas, Nano Lett. **17**, 2647 (2017)
8. J. Lee, M. Tymchenko, C. Argyropoulos, P.-Y. Chen, F. Lu, F. Demmerle, G. Boehm, M.-C. Amann, A. Alù, M.A. Belkin, Giant nonlinear response from plasmonic metasurfaces coupled to intersubband transitions, Nature (London) **511**, 65 (2014)
9. F. Wang, A.B.F. Martinson, H. Harutyunyan, Efficient nonlinear metasurface based on nonplanar plasmonic nanocavities, ACS Photonics **4**, 1188 (2017)
10. A. Noor, A.R. Damodaran, I.-H. Lee, S.A. Maier, S.-H. Oh, C. Ciracì, Mode-matching enhancement of second-harmonic generation with plasmonic nanopatch antennas, ACS Photonics **7**, 3333 (2020)
11. M. Hentschel, B. Metzger, B. Knabe, K. Buse, H. Giessen, Linear and nonlinear optical properties of hybrid metallic–dielectric plasmonic nanoantennas, Beilstein J. Nanotechnol. **7**, 111 (2016)
12. E. Barakat, M.-P. Bernal, F.I. Baida, Theoretical analysis of enhanced nonlinear conversion from metallo-dielectric nanostructures, Opt. Express **20**, 16258 (2012)
13. J. Deng, Y. Tang, S. Chen, K. Li, A.V. Zayats, G. Li, Giant enhancement of second-order nonlinearity of epsilon-nearzero medium by a plasmonic metasurface, Nano Lett. **20**, 5421 (2020)
14. M.P. Nielsen, X. Shi, P. Dichtl, S.A. Maier, R.F. Oulton, Giant nonlinear response at a plasmonic nanofocus drives efficient four-wave mixing, Science **358**, 1179 (2017)
15. A.V. Krasavin, P. Ginzburg, A.V. Zayats, Free-electron optical nonlinearities in plasmonic nanostructures: A review of the hydrodynamic description, Laser Photon. Rev. **12**, 1700082 (2018)
16. A. Chizmeshya, E. Zaremba, Second-harmonic generation at metal surfaces using an extended Thomas Fermi von Weizsacker theory, Phys. Rev. B **37**, 2805 (1988)
17. N. Crouseilles, P.-A. Hervieux, G. Manfredi, Quantum hydrodynamic model for the nonlinear electron dynamics in thin metal films, Phys. Rev. B **78**, 155412 (2008)
18. M. Scalora, M.A. Vincenti, D. de Ceglia, V. Roppo, M. Centini, N. Akozbek, M.J. Bloemer, Second- and third-harmonic generation in metal-based structures, Phys. Rev. A **82**, 043828 (2010)
19. Y. Pavlyukh, J. Berakdar, W. Hubner, Semi – classical approximation for second-harmonic generation in nanoparticles, New J. Phys. **14**, 093044 (2012)
20. C. Ciracì, E. Poutrina, M. Scalora, D.R. Smith, Origin of second-harmonic generation enhancement in optical split-ring resonators, Phys. Rev. B **85**, 201403 (2012)
21. A. Boltasseva, H.A. Atwater, Low-loss plasmonic metamaterials, Science **331**, 290 (2011)
22. G.V. Naik, V.M. Shalaev, A. Boltasseva, Alternative plasmonic materials: beyond gold and silver, Adv. Mater. **25**, 3264 (2013)
23. T. Taliercio, P. Biagioni, Semiconductor infrared plasmonics, Nanophotonics **8**, 949 (2019)
24. Y. Su, W. Wang, X. Hu, H. Hu, X. Huang, Y. Wang, J. Si, X. Xie, B. Han, H. Feng, Q. Hao, G. Zhu, T. Duan, W. Zhao, 10 Gbps DPSK transmission over free-space link in the midinfrared, Opt. Express **26**, 34515 (2018)
25. F. De Luca, M. Ortolani, C. Ciracì, Free electron nonlinearities in heavily doped semiconductors plasmonics, Phys. Rev. B **103**, 115305 (2021)
26. W. Yan, Hydrodynamic theory for quantum plasmonics: linear response dynamics of the inhomogeneous electron gas, Phys. Rev. B **91**, 115416 (2015)
27. D. de Ceglia, M. Scalora, M.A. Vincenti, S. Campione, K. Kelley, E.L. Runnerstrom, J.-P. Maria, G.A. Keeler, and T.S. Luk, Viscoelastic optical nonlocality of low-loss epsilon-nearzero nanofilms, Sci. Rep. **8**, 9335 (2018)
28. S. Raza, S.I. Bozhevolnyi, M. Wubs, N.A. Mortensen, Nonlocal optical response in metallic nanostructures, J. Phys.: Condens. Matter **27**, 183204 (2015)
29. C. Ciracì, F. Della Sala, Quantum hydrodynamic theory for plasmonics: impact of the electron density tail, Phys. Rev. B **93**, 205405 (2016)
30. COMSOL MULTIPHYSICS, www.comsol.com.
31. F. De Luca, C. Ciracì, Difference-frequency generation in plasmonic nanostructures: A parameter-free hydrodynamic description, J. Opt. Soc. Am. B **36**, 1979 (2019)
32. M. Celebrano, X. Wu, M. Baselli, S.G. Mann, P. Biagioni, A. Locatelli, C. de Angelis, G. Cerullo, R. Osellame, B. Hecht, L. Duò, F. Ciccacci, M. Finazzi, Mode matching in multiresonant plasmonic nanoantennas for enhanced second harmonic generation, Nat. Nanotechnol. **10**, 412 (2015)

33. M. Celebrano, A. Locatelli, L. Ghirardini, G. Pellegrini, P. Biagioni, A. Zilli, X. Wu, S. Grossmann, L. Carletti, C. De Angelis, L. Duò, B. Hecht, M. Finazzi, Evidence of cascaded third-harmonic generation in noncentrosymmetric gold nanoantennas, Nano Lett. **19**, 7013 (2019).
34. F. De Luca, M. Ortolani, C. Ciracì, Free electron cascaded third-harmonic generation, 15th International Congress on Artificial Materials for Novel Wave Phenomena - Metamaterials (2021)
35. R.W. Boyd, Nonlinear Optics (Academic, San Diego, 2006)
36. S.M. Sze, Physics of Semiconductor Devices (John Wiley and Sons, Inc, New York, 1981)
37. J.L. Humphrey, D. Kuciauskas, Optical susceptibilities of supported indium tin oxide thin films, J. Appl. Phys. **100**, 113123 (2006)
38. J.R. Maack, N.A. Mortensen, M. Wubs, Size-dependent nonlocal effects in plasmonic semiconductor particles, Europhys. Lett. **119**, 17003 (2021)
39. S.S. Jha, N. Bloembergen, Nonlinear optical susceptibilities in group-IV and III-V semiconductors, Phys. Rev. **171**, 891 (1968)

Cite this article as: Federico De Luca, Michele Ortolani, Cristian Ciracì, Free electron harmonic generation in heavily doped semiconductors: the role of the materials properties, EPJ Appl. Metamat. **9**, 13 (2022)